Letter

Single-Photon-Compatible Telecommunications-Band Quantum Memory in a Hot Atomic Gas

S.E. Thomas,[1] S. Sagona-Stophel,[1] Z. Schofield,[2] I.A. Walmsley,[1] and P.M. Ledingham[2,*]

[1] *QOLS, Department of Physics, Imperial College London, London SW7 2BW, United Kingdom*

[2] *Department of Physics and Astronomy, University of Southampton, Southampton SO17 1BJ, United Kingdom*

(Received 8 November 2022; revised 11 February 2023; accepted 15 February 2023; published 16 March 2023)

The efficient storage and on-demand retrieval of quantum optical states that are compatible with the telecommunications band is a requirement for future terrestrial-based quantum optical networking. Spectrum in the telecommunications band minimizes optical fiber-propagation losses, and broad optical bandwidth facilitates high-speed networking protocols. Here we report on a telecommunications-wavelength- and bandwidth-compatible quantum memory. Using the Off-Resonant Cascaded Absorption protocol in hot ^{87}Rb vapor, we demonstrate a total internal memory efficiency of 20.90(1)% with a Doppler-limited storage time of 1.10(2) ns. We characterize the memory performance with weak coherent states and measure a signal-to-noise ratio of $1.9(1) \times 10^4$ for an average input photon number of 0.084.

DOI: 10.1103/PhysRevApplied.19.L031005

Introduction—Quantum light-matter interfaces are a critical component for quantum repeating [1,2] technology and therefore building large-scale quantum networks [3–5]. Such interfaces allow for a quantum memory [6], a device capable of storing true single photons with both high fidelity and efficiency, with on-demand retrieval after a sufficiently long storage time. Besides these important attributes, compatibility with wavelengths in the telecommunications band, as well as gigahertz operational bandwidth, is of crucial importance to allow high-repetition-rate quantum photonic operations in low-loss optical fiber networks.

Significant progress has been made in realizing telecom quantum optical memories across different material platforms. Atomic-based systems require an optical transition in the telecom range, with cryogenically cooled trivalent erbium ions in solid-state hosts a popular choice [7]. Protocols including the atomic frequency comb (AFC) [8–10], stark-modulated AFC [11,12], controlled-reversible inhomogeneous broadening [13], and revival of silenced echo [14] have been performed in erbium-doped Y_2SiO_5; this includes realizations in nanophotonic structures [9,11]. Other hosts have been explored, with demonstrations of AFC in erbium-doped optical fiber [15,16] and lithium niobate waveguides [17]. Further, frequency conversion via nonlinear processes have been used to interface telecom light with quantum memories, including four-wave mixing in cold atomic clouds [18,19] and nonlinear crystals [20,21]. Furthermore, optomechanical interactions have enabled telecom light storage in optical fiber [22], chalcogenide glass chips [23], and nanofabricated mechanical resonators [24].

Despite these impressive advances, the combination of on-demand readout with high signal-to-noise ratio (SNR) remains elusive. Erbium-based systems suffer poor optical pumping leading to high absorbing backgrounds that limit the overall memory efficiency [13], requiring magnetic fields of the order of 7 T and a 2 K temperature to overcome [10]. Frequency conversion adds layers of inefficiency, and in the case of nonlinear crystals adds noise via pump-induced Raman scattering and spurious spontaneous parametric down-conversion [25]. Optomechanical systems need to overcome the challenge of reaching the mechanical quantum ground state to remove thermal-phononic-mode-induced noise [26]. In this work, we circumvent these problems and demonstrate an ultra-low-noise, high-bandwidth quantum memory using a telecom transition in hot rubidium vapor.

Protocol—We use the off-resonant cascaded absorption (ORCA) [27] protocol for our demonstration. ORCA comprises two counterpropagating optical fields that are two-photon resonant with an optical ladder transition of an atomic ensemble while being detuned from the intermediate transition by Δ (Fig. 1), giving rise to absorption of the beams by exciting the atoms in the ensemble. The intense control pulse dresses the atomic system, providing a broad virtual state to which the signal field couples efficiently, so that it may be completely absorbed. For large enough intermediate detuning, the absorption bandwidth is determined by the bandwidth of the control pulse. The input pulse excites a superposition of atoms in the

*P.Ledingham@soton.ac.uk

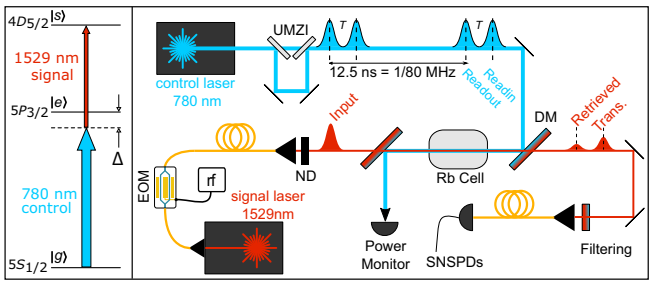

FIG. 1. Left: Telecom ORCA-level scheme. Right: Experimental setup. DM, dichroic mirror; ND, neutral density filters; RF, arbitrary waveform generator; SNSPD, superconducting nanowire single-photon detectors; UMZI, unbalanced Mach–Zehnder interferometer.

ensemble of the $|g\rangle$-$|s\rangle$ transition. The state of the atomic ensemble after absorption of the signal is of the form $(1/\sqrt{N})\ \sum_{j=1}^{N}\ \exp\left[i(\vec{k}_s - \vec{k}_c)\cdot\vec{v}_j t\right]\ |g_1,\ldots,s_j,\ldots,g_N\rangle$ where $|g(s)_j\rangle$ labels the ground (storage) state of the jth atom, N is the total number of atoms, $\vec{k}_{s(c)}$ is the input (control) pulse wave vector, and $\vec{v}_j$ is the velocity of the jth atom. The collective dipole moment will emit light upon the application of a second control pulse after a storage time T, allowing the signal to be read out and completing the memory operation.

The main benefits of ORCA are threefold. Firstly, the optical fields can be at significantly different wavelengths, depending on the chosen atomic species and on the levels used. This makes it simple to filter the strong control from the single-photon-level signal. Secondly, the storage state is a doubly excited one and so has no atomic population under normal operational conditions. This simplifies the approach by not needing any initialization of the atomic ensemble with optical pumping fields, and eliminates spontaneous emission noise associated with inefficient optical pumping. Finally, four-wave mixing type noise is eliminated. For example, in Lambda-based approaches, the strong control is able to efficiently Raman scatter from the populated ground state, spontaneously emitting a photon and leaving spurious excitations in the storage state that are subsequently read out into the same spatial-spectral-temporal mode as that of the desired signal [28]. Equivalent processes with a ladder system are not possible. In the case of a nondegenerate ladder system, there is no two-control-photon process that can populate the storage state and so the ORCA protocol is inherently noise-free in this respect.

ORCA has been achieved in hot atomic vapors demonstrating low-noise operation over the gigahertz bandwidth allowing for high SNR for single-photon-level inputs [29], recall of heralded single photons [27], and can be used as a time-nonstationary coherent spectral-temporal filter to improve indistinguishably of single photon sources [30]. Here we extend the ORCA protocol to store light in the telecom-band.

Experimental setup—Fig. 1 shows the experimental setup. An ensemble of rubidium atoms in a cell of length 8 cm is heated to around 120 °C, yielding an optical depth of 8510, with a Doppler broadened linewidth of 585 MHz, found by fitting a measured spectrum using a scanning laser on the D2 line with the Elecsus software [31]. We estimate the vapor to contain 96.9% of the isotope ^{87}Rb. The ladder system used for this demonstration is depicted in the left panel of Fig. 1. We utilize the doubly excited $4D_{5/2}$ state as the storage state $|s\rangle$, which connects to the ground state $|g\rangle$ $(5P_{1/2},\ F = 2)$ via a two-photon process with the telecommunication-band-compatible wavelength 1529.3 nm (signal) and the Rb D2 line at 780.3 nm (control). The signal (control) field is blue-detuned (red-detuned) from the intermediate level $|e\rangle$ $(5P_{3/2}, F' = \{1, 2, 3\})$ by $\Delta = 6$ GHz.

Control pulses of a few nanojoules energy are delivered by a mode-locked Titanium Sapphire laser (Spectra Physics Tsunami) at a repetition rate of 80 MHz. The pulse bandwidth is approximately 1 GHz. An unbalanced Mach–Zehnder interferometer (UMZI) splits an individual pulse into the readin and readout pulses, separated by time T. We use polarizing beamsplitters to construct the UMZI, with a half waveplate before used to adjust the energy into each of the pulses. The output of the UMZI is polarized by a half waveplate and polarizing beamsplitter (PBS) (not shown), to ensure that the readin and readout control pulses have the same polarization. Dichroic mirrors are used to overlap and separate the control and the signal mode, and we monitor the average power of the control pulses with a power meter (Thorlabs). The signal is generated from a continuous-wave telecom laser (Santec) that is passed through an intensity modulator (iXBlue) driven by a fast arbitrary waveform generator (Tektronix) to generate gigahertz-bandwidth Gaussian pulses of around 300 ps duration synchronized to the repetition rate of the control pulse laser and delivered at a rate of 10 MHz. Neutral density filters are used to reduce the intensity of the pulses to the single-photon level. High- transmission-band and long-pass filters are placed before the detection fiber to provide 14-orders- of-magnitude suppression of background light at the control pulse wavelength. Photons are detected with superconducting nanowire single-photon detectors (Photon Spot) together with a time-to-digital converter (Swabian) to produce start-stop histograms.

Memory performance—Figure 2(a) shows a plot of storage and recall of telecom light for the highest measured storage efficiency. We implement Gaussian fits to these traces and use these fits to calculate photon number and efficiencies. We use an input pulse with an average number of photons per pulse of $\mu_{\text{in}} = 0.084(10)$. The mean photon number

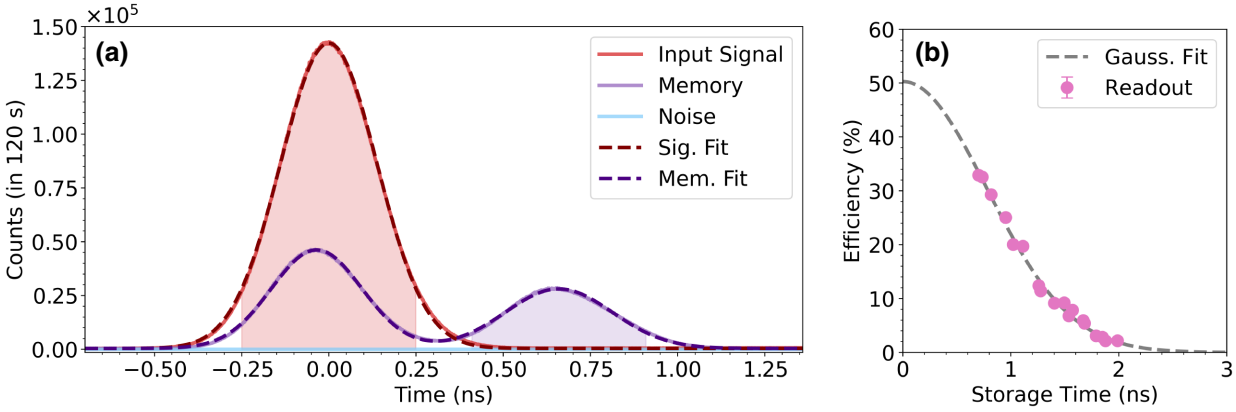

FIG. 2. (a) Storage and retrieval of telecom light. The solid lines are the start-stop histograms for the signal at input (red), at the memory output (purple) and the noise without signal (light blue); the timing resolution of the time-to-digital converter (TDC) is 1 ps and the measurement time for each data set is 120 s. The dashed lines show Gaussian fits to the measured signal. The shaded areas indicate the readin and readout integration windows of 500 ps width. The storage time in this case is 660 ps. (b) Readout efficiency vs storage time. Pink circles are the data which are fitted with a Gaussian function of control delay (gray dashed line). For these data, the measurement time per data point is 10 s, with integration window as before.

was estimated by integrating the counts over a 500-ps integration window centered on the 350-ps full width at half maximum pulse at $t = 0$, then dividing out detection loss ($\eta_{\text{det}} = 80(8)\%$) and transmission from the input of the cell to the detector ($\eta_{\text{trans}} = 56(4)\%$), and finally normalizing by the number of trials in the 120 s total measurement time. Two control pulses, with a time separation of 660 ps, are applied to read in and read out the signal to the memory, with respective energies of 0.57(4) nJ and 3.6(3) nJ. When photons are successfully stored, they are measured in the time region called the "readout window," while photons that are not successfully stored pass through undelayed by the memory in the "readin window." We define the readin efficiency as the proportion of light that is read in to the memory, or 1 minus the number of counts remaining in the readin window when the control field is on compared to the input state when the control field is off; in this case it is $\eta_{\text{readin}} = 69.13(1)\%$. We see clear retrieved signal in the readout window, defined as the 500-ps window centered at $t = 660$ ps. The total internal memory efficiency, defined as the ratio of readout to input counts, is measured to be $\eta_{\text{mem}} = 20.90(1)\%$, resulting in a readout efficiency of $\eta_{\text{readout}} = 30.23(1)\%$. The total throughput efficiency for the input at the front of the cell to being stored, retrieved, and detected is $\eta_{\text{mem}}\eta_{\text{trans}}\eta_{\text{det}} = 9.4(1.2)\%$.

Storage dynamics—Figure 2(b) shows the readout memory efficiency as a function of readout delay after the storage. Performed under similar conditions to Fig. 2(a), we measure an average readin efficiency of $\eta_{\text{readin}} = 78(2)\%$ and infer the readout efficiency at zero storage time from the fit to be $\eta_{\text{readout}} = 50(2)\%$. The readin and readout efficiencies are not matched. Forward retrieval (i.e., the retrieved signal propagates in the same direction as the input) results in reabsorption of the signal toward the exit of the cell, reducing the maximum efficiency for fixed control pulse energy. Backward retrieval can, in principle, avoid this [32].

The characteristic lifetime of 1.10(2) ns is extracted from a Gaussian fit. The lifetime is limited by inhomogeneous Doppler broadening of the atoms causing dephasing of the atomic polarization. Atom j constituting the collective dipole moment between the ground and storage state has a net wavevector $\exp[i(\vec{k}_s - \vec{k}_c) \cdot \vec{v}_j t]$, where $(\vec{k}_s - \vec{k}_c) \cdot \vec{v}_j$ is the Doppler shift for the jth atom. Given the broad Maxwell-Boltzmann distribution of velocities of the atomic vapor, each atom accumulates a different phase, thereby reducing the collective dipole moment. The spatial wavelength of the collective orbital-wave excitation is around 1.6 μm, a distance traversed by an atom in the hot vapor in a few nanoseconds. The storage time is also reduced by the interference of multiple pathways through different hyperfine states with characteristic time scales of around 10 ns [27]. The natural lifetime of the storage state provides the ultimate limit of around 90 ns [33,34]. The time scale we have measured here is consistent with that expected from Doppler dephasing [35], suggesting strongly that this is the main limitation for our storage time.

Control dependence—The data presented in Fig. 2 show the optimized output efficiency. The ORCA memory efficiency varies with the total energy in the control pulses, and is shown for a readout to readin ratio, $\mathcal{R} = E_{R_{\text{out}}}/E_{R_{\text{in}}}$, of $\mathcal{R} = 3.3(1)$ in Fig. 3. Note that this is a different condition for Fig. 2 with $\mathcal{R} = 6.4(1)$, allowing for more pulse energy for the readin process (and so less for the readout). The readin efficiency quickly increases and then begins

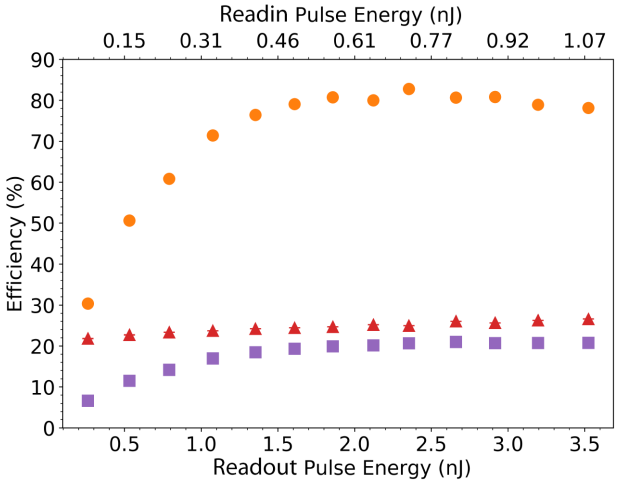

FIG. 3. ORCA memory versus pulse energy. Plot shows readin efficiency (orange circles), readout efficiency (red triangles) and total internal memory efficiency (purple squares) for different energies in readin and readout control pulses for $\mathcal{R} = 3.3(1)$. For this data, the measurement time per data point is 10 s and the integration window is 500 ps.

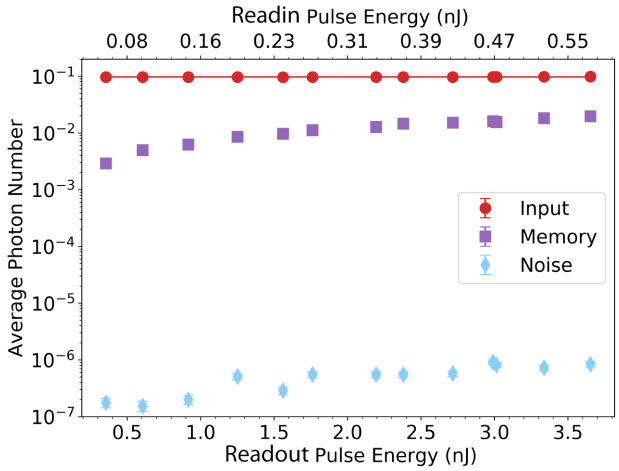

FIG. 4. The average photon number per integration bin for the input (red circles), memory (purple squares) and noise (light blue diamonds) as a function of control pulse energy. For these data, $\mathcal{R} = 6.4(1)$, the measurement time per data point is 10 s, and the integration window is 500 ps.

to decrease when the readin pulse energy is near 0.7 nJ. This decrease is the consequence of the ac-Stark effect by which the atomic resonances are frequency-shifted by the control pulse. The effect scales as Ω^2/Δ, where Ω is the Rabi frequency of the control field, and so higher control pulse energies result in shifts large enough to move the optical fields out of two-photon resonance and reduce the efficiency. One approach to preventing this is to optimize the spectral-temporal mode of the control pulse for a given pulse energy [36,37]. This effect is not seen on the readout efficiency because the optical mode that is read out will frequency shift with the atoms.

Noise performance—A critical requirement for any quantum memory is that the output SNR be sufficiently high to retain the input quantum state upon readout. In Fig. 4 we assess the SNR by quantifying the average number of photons per pulse in the input, the retrieved output, and the noise floor (when the input signal is blocked but the control pulses are switched on) for $\mathcal{R} = 6.4$. We measure the noise floor to be less than 10^{-6} photons per cycle. There is a slight linear increase of the noise as a function of control pulse energy which we attribute to leakage either of the control pulse or of one-photon scattering events of the control with the atoms. In spite of this we observe an SNR of around 10^4 for every control pulse energy tested using μ_{in} at about 0.1. For the data in Fig. 2(a) with input photon number 0.084 we measure the SNR to be $1.9(1) \times 10^4$.

A useful metric to compare the performance of quantum memories is the ratio of the noise counts on the output to the total internal memory efficiency: $\mu_1 = N/\eta_{\text{mem}}$ [38]. This parameter μ_1 is essentially the number of photons per pulse on average at the input of the quantum memory that gives an SNR of 1 at the output. For the data in Fig. 2(a) we measure the noise to be $N = 9(1) \times 10^{-7}$ photons per pulse over the integration window of 500 ps. This leads to $\mu_1 = 4.5(6) \times 10^{-6}$, which is approximately a one-order-of-magnitude improvement compared to the previous ORCA demonstrations [27,29,30], due to the low dark count rate of superconducting nanowire detectors. To our knowledge this is the lowest reported for atom-based quantum memories.

We can infer the quantum performance this memory could achieve. The second-order coherence of a retrieved single photon from the memory for a given μ_{in} and $g^{(2)}_{\text{in}}$ is given by

$$g^{(2)}_{\text{out}} = \frac{(\mu_{\text{in}}/\mu_1)^2 g^{(2)}_{\text{in}} + 2(\mu_{\text{in}}/\mu_1 + 1)}{(\mu_{\text{in}}/\mu_1 + 1)^2},$$

under the assumption that the noise is thermal, and is created independently of the memory process, so that the output can be treated as an incoherent admixture of signal and noise [28]. Furthermore, the output fidelity for single-photon storage follows $F = (\mu_{\text{in}} + \mu_1)/(\mu_{\text{in}} + 2\mu_1)$ [38]. For an ideal single-photon source with $\mu_{\text{in}} = 1$ and $g^{(2)}_{\text{in}} = 0$, our ORCA memory would retrieve the photon with $g^{(2)} = 9(1) \times 10^{-6}$ and the retrieved qubit fidelity would be at the 99.9996% level. For the case of a far-from-ideal source with $\mu_{\text{in}} = 0.01$ and $g^{(2)}_{\text{in}} = 0.2$, the memory would retrieve the photon with $g^{(2)}_{\text{out}} = g^{(2)}_{\text{in}} + 7.2 \times 10^{-4}$ and $F = 99.96\%$.

Discussion—Our telecommunication-wavelength ORCA quantum memory has demonstrated exceptional SNR performance over a gigahertz bandwidth. This opens up

the possibility of interfacing with single-photon sources based on parametric-down-conversion or four-wave mixing with modest spectral filtering to match our memory bandwidth, as well as to (In,Ga)As quantum-dot photon sources [39,40] the bandwidths of which are well matched to our device. Total memory efficiencies approaching unity should be achieved with optimal temporal-spectral mode shaping of the control pulse [27,30,41]. For some applications, the limitation of our memory is the Doppler-induced storage time, as discussed previously. Magneto-optical trapping of the ensemble would eliminate atomic motion, albeit with the additional complexity of ultrahigh-vacuum chambers. An alternative approach to eliminating the dephasing is to perform velocity-selective optical pumping (VSP) to target atoms with a narrow spread of velocities [35] or even tailor atomic frequency comb structures for rephasing [42]. However, these trapped and VSP approaches sacrifice significant atom numbers and therefore total memory efficiency. An approach that utilizes all atoms is to apply additional optical fields that compensate the dephasing by means of a controlled dynamic ac-Stark shift [43], or using additional optical fields to map to an auxiliary state in order to facilitate a backward read out that would automatically undo the accumulated phase [44]. With Doppler-dephasing eliminated, the storage time would be limited to the decay time of the $4D_{5/2}$ state, of around 90 ns. Overcoming this would require additional fields to map to longer-lived states (e.g. a higher-lying Rydberg state) or to ground state.

Conclusion—We present a gigahertz-bandwidth quantum memory for telecom-band light. We demonstrate a total efficiency of 20.90(1)% and a lifetime of 1.10(2) ns. The noise performance is unprecedented with a measured SNR of $1.9(1) \times 10^4$ for $\mu_{\text{in}} = 0.084$, which could allow for input states with an average photon number as low as $4.5(6) \times 10^{-6}$ to yield an SNR equal to 1. We discuss avenues for further improvements on both storage time and efficiency, which would fulfill a critical requirement for future quantum technologies.

Acknowledgments—This work was supported by the Engineering and Physical Sciences Research Council via the Quantum Computing and Simulation Hub (T001062) and the Horizon 2020 research and innovation program under Grant Agreement No. 899814 (Qurope). P.M.L. acknowledges a UKRI Future Leaders Fellowship Grant Reference MR/V023845/1.

[1] H.-J. Briegel, W. Dür, J. I. Cirac, and P. Zoller, Quantum Repeaters: The Role of Imperfect Local Operations in Quantum Communication, Phys. Rev. Lett. **81**, 5932 (1998).

[2] N. Gisin and R. Thew, Quantum communication, Nat. Photon. **1**, 165 (2007).

[3] T. D. Ladd, F. Jelezko, R. Laflamme, Y. Nakamura, C. Monroe, and J. L. O'Brien, Quantum computing, Nature **464**, 45 (2010).

[4] P. Kómár, E. M. Kessler, M. Bishof, L. Jiang, A. S. Sørensen, J. Ye, and M. D. Lukin, A quantum network of clocks, Nat. Phys. **10**, 582 (2014).

[5] S. Wehner, D. Elkouss, and R. Hanson, Quantum internet: A vision for the road ahead, Science **362**, 641 (2018).

[6] K. Heshami, D. G. England, P. C. Humphreys, P. J. Bustard, V. M. Acosta, J. Nunn, and B. J. Sussman, Quantum memories: Emerging applications and recent advances, J. Mod. Opt. **63**, 2005 (2016).

[7] Y. C. Sun, *Rare Earth Materiais in Optical Storage and Data Processing Applications* (Springer, Berlin, 2005), p. 379.

[8] B. Lauritzen, J. c. v. Minář, H. de Riedmatten, M. Afzelius, and N. Gisin, Approaches for a quantum memory at telecommunication wavelengths, Phys. Rev. A **83**, 012318 (2011).

[9] I. Craiciu, M. Lei, J. Rochman, J. M. Kindem, J. G. Bartholomew, E. Miyazono, T. Zhong, N. Sinclair, and A. Faraon, Nanophotonic Quantum Storage at Telecommunication Wavelength, Phys. Rev. Appl. **12**, 024062 (2019).

[10] J. S. Stuart, M. Hedges, R. Ahlefeldt, and M. Sellars, Initialization protocol for efficient quantum memories using resolved hyperfine structure, Phys. Rev. Res. **3**, L032054 (2021).

[11] I. Craiciu, M. Lei, J. Rochman, J. G. Bartholomew, and A. Faraon, Multifunctional on-chip storage at telecommunication wavelength for quantum networks, Optica **8**, 114 (2021).

[12] D.-C. Liu, P.-Y. Li, T.-X. Zhu, L. Zheng, J.-Y. Huang, Z.-Q. Zhou, C.-F. Li, and G.-C. Guo, On-Demand Storage of Photonic Qubits at Telecom Wavelengths, Phys. Rev. Lett. **129**, 210501 (2022).

[13] B. Lauritzen, J. c. v. Minář, H. de Riedmatten, M. Afzelius, N. Sangouard, C. Simon, and N. Gisin, Telecommunication-Wavelength Solid-State Memory at the Single Photon Level, Phys. Rev. Lett. **104**, 080502 (2010).

[14] J. Dajczgewand, J.-L. L. Gouët, A. Louchet-Chauvet, and T. Chanelière, Large efficiency at telecom wavelength for optical quantum memories, Opt. Lett. **39**, 2711 (2014).

[15] J. Jin, E. Saglamyurek, M. l. G. Puigibert, V. Verma, F. Marsili, S. W. Nam, D. Oblak, and W. Tittel, Telecom-Wavelength Atomic Quantum Memory in Optical Fiber for Heralded Polarization Qubits, Phys. Rev. Lett. **115**, 140501 (2015).

[16] S.-H. Wei, B. Jing, X.-Y. Zhang, J.-Y. Liao, H. Li, L.-X. You, Z. Wang, Y. Wang, G.-W. Deng, H.-Z. Song, D. Oblak, G.-C. Guo, and Q. Zhou, Storage of 1650 modes of single photons at telecom wavelength. arXiv:2209.00802 (2022).

[17] M. F. Askarani, M. G. Puigibert, T. Lutz, V. B. Verma, M. D. Shaw, S. W. Nam, N. Sinclair, D. Oblak, and W. Tittel, Storage and Reemission of Heralded Telecommunication-Wavelength Photons Using a Crystal Waveguide, Phys. Rev. Appl. **11**, 054056 (2019).

[18] A. G. Radnaev, Y. O. Dudin, R. Zhao, H. H. Jen, S. D. Jenkins, A. Kuzmich, and T. A. B. Kennedy, A quantum memory with telecom-wavelength conversion, Nat. Phys. **6**, 894 (2010).

[19] D.-S. Ding, Z.-Y. Zhou, B.-S. Shi, X.-B. Zou, and G.-C. Guo, Storage and retrieval of a light in telecomband in a cold atomic ensemble. arXiv:1210.3963 (2012).

[20] N. Maring, K. Kutluer, J. Cohen, M. Cristiani, M. Mazzera, P. M. Ledingham, and H. de Riedmatten, Storage of up-converted telecom photons in a doped crystal, New J. Phys. **16**, 113021 (2014).

[21] X.-Y. Luo, Y. Yu, J.-L. Liu, M.-Y. Zheng, C.-Y. Wang, B. Wang, J. Li, X. Jiang, X.-P. Xie, Q. Zhang, X.-H. Bao, and J.-W. Pan, Entangling metropolitan-distance separated quantum memories, Nature **578**, 240 (2020).

[22] Z. Zhu, D. J. Gauthier, and R. W. Boyd, Stored light in an optical fiber via stimulated brillouin scattering, Science **318**, 1748 (2007).

[23] M. Merklein, B. Stiller, K. Vu, S. J. Madden, and B. J. Eggleton, A chip-integrated coherent photonic-phononic memory, Nat. Comms. **8**, 574 (2017).

[24] A. Wallucks, I. Marinković, B. Hensen, R. Stockill, and S. Gröblacher, A quantum memory at telecom wavelengths, Nat. Phys. **16**, 772 (2020).

[25] J. S. Pelc, L. Ma, C. R. Phillips, Q. Zhang, C. Langrock, O. Slattery, X. Tang, and M. M. Fejer, Long-wavelength-pumped upconversion single-photon detector at 1550 nm: Performance and noise analysis, Opt. Express **19**, 21445 (2011).

[26] P. K. Shandilya, D. P. Lake, M. J. Mitchell, D. D. Sukachev, and P. E. Barclay, Optomechanical interface between telecom photons and spin quantum memory, Nat. Phys. **17**, 1420 (2021).

[27] K. T. Kaczmarek, P. M. Ledingham, B. Brecht, S. E. Thomas, G. S. Thekkadath, O. Lazo-Arjona, J. H. D. Munns, E. Poem, A. Feizpour, D. J. Saunders, J. Nunn, and I. A. Walmsley, High-speed noise-free optical quantum memory, Phys. Rev. A **97**, 042316 (2018).

[28] S. E. Thomas, T. M. Hird, J. H. D. Munns, B. Brecht, D. J. Saunders, J. Nunn, I. A. Walmsley, and P. M. Ledingham, Raman quantum memory with built-in suppression of four-wave-mixing noise, Phys. Rev. A **100**, 033801 (2019).

[29] R. Finkelstein, E. Poem, O. Michel, O. Lahad, and O. Firstenberg, Fast, noise-free memory for photon synchronization at room temperature, Sci. Adv. **4**, eaap8598 (2018).

[30] S. Gao, O. Lazo-Arjona, B. Brecht, K. T. Kaczmarek, S. E. Thomas, J. Nunn, P. M. Ledingham, D. J. Saunders, and I. A. Walmsley, Optimal Coherent Filtering for Single Noisy Photons, Phys. Rev. Lett. **123**, 213604 (2019).

[31] M. A. Zentile, J. Keaveney, L. Weller, D. J. Whiting, C. S. Adams, and I. G. Hughes, Elecsus: A program to calculate the electric susceptibility of an atomic ensemble, Comput. Phys. Commun. **189**, 162 (2015).

[32] K. Surmacz, J. Nunn, K. Reim, K. C. Lee, V. O. Lorenz, B. Sussman, I. A. Walmsley, and D. Jaksch, Efficient spatially resolved multimode quantum memory, Phys. Rev. A **78**, 033806 (2008).

[33] C. E. Theodosiou, Lifetimes of alkali-metal—atom Rydberg states, Phys. Rev. A **30**, 2881 (1984).

[34] M. S. Safronova, C. J. Williams, and C. W. Clark, Relativistic many-body calculations of electric-dipole matrix elements, lifetimes, and polarizabilities in rubidium, Phys. Rev. A **69**, 022509 (2004).

[35] D. Main, T. M. Hird, S. Gao, E. Oguz, D. J. Saunders, I. A. Walmsley, and P. M. Ledingham, Preparing narrow velocity distributions for quantum memories in room-temperature alkali-metal vapors, Phys. Rev. A **103**, 043105 (2021).

[36] J. Nunn, I. A. Walmsley, M. G. Raymer, K. Surmacz, F. C. Waldermann, Z. Wang, and D. Jaksch, Mapping broadband single-photon wave packets into an atomic memory, Phys. Rev. A **75**, 011401 (2007).

[37] A. V. Gorshkov, A. André, M. Fleischhauer, A. S. Sørensen, and M. D. Lukin, Universal Approach to Optimal Photon Storage in Atomic Media, Phys. Rev. Lett. **98**, 123601 (2007).

[38] M. Gündoğan, P. M. Ledingham, K. Kutluer, M. Mazzera, and H. De Riedmatten, Solid State Spin-Wave Quantum Memory for Time-Bin Qubits, Phys. Rev. Lett. **114**, 1 (2015).

[39] S. Kolatschek, C. Nawrath, S. Bauer, J. Huang, J. Fischer, R. Sittig, M. Jetter, S. L. Portalupi, and P. Michler, Bright Purcell enhanced single-photon source in the telecom O-band based on a quantum dot in a circular Bragg grating, Nano Lett. **21**, 7740 (2021).

[40] T. Lettner, S. Gyger, K. D. Zeuner, L. Schweickert, S. Steinhauer, C. Reuterskiöld Hedlund, S. Stroj, A. Rastelli, M. Hammar, R. Trotta, K. D. Jöns, and V. Zwiller, Strain-controlled quantum dot fine structure for entangled photon generation at 1550 nm, Nano Lett. **21**, 10501 (2021).

[41] J. Guo, X. Feng, P. Yang, Z. Yu, L. Q. Chen, C.-H. Yuan, and W. Zhang, High-performance raman quantum memory with optimal control in room temperature atoms, Nat. Commun. **10**, 148 (2019).

[42] D. Main, T. M. Hird, S. Gao, I. A. Walmsley, and P. M. Ledingham, Room temperature atomic frequency comb storage for light, Opt. Lett. **46**, 2960 (2021).

[43] R. Finkelstein, O. Lahad, I. Cohen, O. Davidson, S. Kiriati, E. Poem, and O. Firstenberg, Continuous Protection of a Collective State from Inhomogeneous Dephasing, Phys. Rev. X **11**, 011008 (2021).

[44] S. A. Moiseev and S. Kröll, Complete Reconstruction of the Quantum State of a Single-Photon Wave Packet Absorbed by a Doppler-Broadened Transition, Phys. Rev. Lett. **87**, 173601 (2001).